Engineering Failure Analysis 138 (2022) 106362

Contents lists available at ScienceDirect

Engineering Failure Analysis

journal homepage: www.elsevier.com/locate/engfailanal

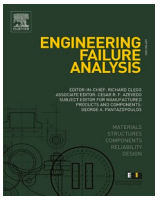

Corrosion-fatigue crack growth behaviour of wire arc additively manufactured ER100S-1 steel specimens

Anna Ermakova [a], Supriyo Ganguly [b], Javad Razavi [c], Filippo Berto [c], Ali Mehmanparast [a,*]

[a] Department of Naval Architecture, Ocean and Marine Engineering, University of Strathclyde, Glasgow G1 1XQ, UK
[b] Welding Engineering and Laser Processing Centre, Cranfield University, Cranfield, MK43 0AL, UK
[c] Norwegian University of Science and Technology (NTNU), Trondheim, Norway

ARTICLE INFO

Keywords:
Corrosion-fatigue
WAAM
Additive manufacturing
Offshore structures
Structural Integrity

ABSTRACT

The wire arc additive manufacturing (WAAM) technology is a promising fabrication technique which has been proven to have many advantages for producing large structures; however, the fatigue and corrosion-fatigue performance of WAAM steel components for application in the marine environments is still unexplored. In this study, the WAAM technique was employed to fabricate four specimens made of ER100S-1 steel, which were then tested under cyclic loading conditions in seawater to assess the corrosion-fatigue crack growth (CFCG) behaviour and hence suitability of this fabrication technology for offshore renewable energy applications. The test duration, cracking mechanisms and CFCG rate were investigated for each specimen and the material's behaviour was investigated by considering the microstructural examinations. Furthermore, the obtained results were compared with the BS7910 standard recommended trends and experimental data available in the literature for conventionally built weldments made of different grades of steel which are commonly used for offshore applications.

1. Introduction

Offshore structures are commonly manufactured onshore by welding steel sections and then transported to marine environments for installation and operation. The welded joints in offshore structures are considered as potential weak spots which are prone to crack initiation and propagation due to high stress concentration and residual stresses effects introduced during the welding process. These structures experience millions of load cycles during their operation in highly corrosive environments, which can lead to corrosion-fatigue failures if suitable inspection and maintenance strategies are not carefully implemented. Furthermore, the welding process causes phase changes in metal that affect the microstructure and crack growth patterns, by introducing crack branching [1]. Previous studies on welded wrought steel specimens extracted from the heat affected zone (HAZ) exhibit a strong dependence of fatigue crack growth (FCG) rates on the welding parameters, metal composition, crack growth region, residual stress magnitude and distribution pattern, and testing environment [2–6]. These studies suggest that the fatigue life of marine structures can be significantly improved by selecting more appropriate materials and manufacturing techniques.

Wire arc additive manufacturing (WAAM) is a rapidly developing technique that has gained substantial attention for fabrication of large-scale components employed in structural applications. Compared with other additive manufacturing (AM) methods, such as

* Corresponding author.
E-mail address: ali.mehmanparast@strath.ac.uk (A. Mehmanparast).

https://doi.org/10.1016/j.engfailanal.2022.106362
Received 3 December 2021; Received in revised form 18 March 2022; Accepted 26 April 2022
Available online 14 May 2022

Nomenclature

a_0	Initial crack length in C(T) specimen
a_i	Instantaneous crack length
$a_{i,p}$	Crack length after pre-fatigue cracking
$a_{f,c}$	Final crack length (using the compliance data)
$a_{f,op}$	Final crack length (using the fracture surface)
B	Total thickness of C(T) specimen
C	Material constant for fatigue crack growth
da/dN	Fatigue crack growth rate
H	C(T) specimen height
K_{max}	Stress intensity factor corresponding to P_{max}
ΔK	Stress intensity factor range
m	Material constant for fatigue crack growth
P_{max}	Maximum load in fatigue cycles
P_{min}	Minimum load in fatigue cycles
R	Load ratio
R^2	Coefficient of determination
W	C(T) specimen width
AM	Additive Manufacturing
B	Bottom
BFS	Back Face Strain measurement technique
BM	Beach Marking
CFCG	Corrosion-fatigue crack growth
C(T)	Compact Tension specimen
CMT	Cold Metal Transfer
EDM	Electrical Discharge Machining
FCG	Fatigue Crack Growth
H	Horizontal
HAZ	Heat Affected Zone
SIF	Stress Intensity Factor
SD	Standard Deviation
T	Top
V	Vertical
WAAM	Wire Arc Additive Manufacturing

powder-based techniques, WAAM is known to be substantially beneficial for lower manufacturing cost, unlimited build envelope, and significantly high deposition rates (3–8 kg/h), which results in reduction of manufacturing lead-time [7–10]. Despite the advantages of this method, the high heat input and non-uniform solidification rates during the WAAM fabrication process lead to microstructural inhomogeneity and mechanical properties anisotropy [11,12]. Nevertheless, WAAM has been already adopted by many industries, including aerospace and automotive, and offers a great potential for other industrial sectors such as offshore renewable energy and particularly offshore wind turbines. However, in order to investigate the suitability of this technique for manufacturing and repair of renewable energy marine structures, the corrosion-fatigue crack growth (CFCG) performance of WAAM built steel components has to be closely examined and compared with the conventionally welded joints. This will help to estimate the remaining lifetime and develop efficient inspection plans for future WAAM built marine structures and components.

The environmental behaviour of ER70S-6 low carbon WAAM built specimens was investigated by Ron et al. [13], which included the corrosion behaviour assessment in salt spray testing, immersion testing, potentiodynamic polarization analysis, and electrochemical impedance spectroscopy. The obtained results from this study showed that the general and stress corrosion resistance of WAAM specimens were comparable with conventional wrought ST-37 steel counterparts, which led to a conclusion that the WAAM process does not cause any weakening in corrosion performance for the considered application. Another study was conducted on austenitic stainless steel WAAM specimens with a similar analysis procedure [14], which confirmed that despite the microstructural differences and variations in mechanical properties, electrochemical performance and stress corrosion susceptibility of the parts were similar to the wrought counterparts. Additionally, some ER70-6 WAAM built specimens were tested in a 3.5% NaCl solution to investigate the effect of microstructure imperfections on corrosion-fatigue performance [15]. The results revealed a reduction in fatigue strength of WAAM specimens, compared with wrought ST-37 specimens, due to the existence of defects that are imposed during WAAM fabrication process, and stimulate corrosion attacks and accelerate fatigue cracking process.

Previous studies demonstrated that corrosion characteristics of WAAM built specimens may differ compared to the wrought counterparts, due to evident microstructural differences imposed by specific manufacturing process. However, the data available in the literature are very limited and do not show any CFCG rates trends for WAAM built low carbon steels, which is required for in-depth

analysis and comprehensive comparison for considering the use of this technology in marine structures. Thus, the present study investigates the CFCG behaviour of ER100S-1 low carbon steel WAAM built specimens in seawater. This research includes the manufacturing of a WAAM wall, CFCG testing on extracted specimens, crack growth monitoring, data collection and analysis, and comparison of the obtained results with the existing data on wrought steels. Moreover, a sensitivity analysis of the corrosion-fatigue response to the built orientation and location of the specimens was conducted and presented in this study, along with the microstructural analysis. The observations from this study prove the suitability of WAAM technique with ER100S-1 steel wires for offshore applications.

2. Material and specimen preparation

One WAAM wall was manufactured for this study using Cold Metal Transfer (CMT) process with Böhler welding ER100S-1 wire [16], the typical composition for which is presented in Table 1. The detailed parameters for CMT-WAAM fabrication process are shown in Table 2. The manufacturing set-up is demonstrated in Fig. 1 in which a CMT power source, a robotic arm, a CMT torch that is supplying the shielding gas and feeding the metal wire, an exhaust fan to remove any generated fumes and excessive heat are demonstrated. The WAAM wall was deposited in the middle of a base plate that was cut from an EN10025 rolled structural steel plate, with dimensions of 420 × 200 × 12 mm [3]. The completed WAAM wall is shown in Fig. 1. An oscillation process was selected [17–18] for fabricating a relatively thick wall with dimensions of length of 355 mm (X-axis in Fig. 1), thickness of 24 mm (Y-axis in Fig. 1) and height of 140 mm (Z-axis in Fig. 1). The base plate was fixed onto the working table with eight clamps before starting the deposition process, to prevent any bending and distortion of the plate due to the high manufacturing temperatures. These clamps were removed once the WAAM wall was completed and cooled down to the ambient temperature.

After completing the deposition of the WAAM wall, four notched compact tension, C(T), specimens were extracted using Electrical Discharge Machining (EDM) method. The specimens were designed in accordance with the ASTM E647 [19] standard with the width of $W = 50$ mm, height of $H = 60$ mm, total thickness of $B = 16$ mm and initial crack length of $a_0 = 17$ mm. The specimens were extracted from two different locations: top (T) and bottom (B) of the wall, and along two different orientations: vertical (V) – where the crack plane is perpendicular to the deposited layers, and horizontal (H) – where the crack plane is parallel to the deposited layers. All four combinations of specimens are presented schematically in Fig. 2(a). For example, the specimen denoted CT-VT, is a C(T) specimen with vertical orientation, from top of the wall. Knife edges were machined at the crack mouth of the specimens as per ASTM 1820 stndard [20] to attach a clip gauge for compliance measurements during fatigue pre-cracking that is required prior to CFCG testing, to introduce an infinitely sharp crack tip ahead of the machined notch. All four specimens were pre-cracked to approximately 20 mm ($a_{i,p}/W = 0.4$) using the load-decreasing approach. The final value of maximum stress intensity factor K_{max} at the end of pre-cracking did not exceed the initial K_{max} at the beginning of the main CFCG tests. For the CFCG tests performed in seawater, the crack was measured using the back face strain measurement technique, which is explained in section 3. Some examples of the specimens prepared for CFCG testing are displayed in Fig. 2(b).

3. Corrosion-fatigue crack growth tests

3.1. Test set-up

CFCG tests were conducted under load-controlled mode using a 100 kN servo hydraulic Instron machine. A sinusoidal cyclic load wave was applied with a constant amplitude of the maximum load $P_{max} = 10$ kN, the load ratio of $R = 0.1$, and frequency of $f = 0.3$ Hz, which is the typical frequency used in corrosion-fatigue analysis for offshore wind turbine structures [21,22]. To imitate free-corrosion condition for testing, 60 L artificial seawater was made according to the ASTM D1141-98 standard [23] using deionised water and a set of chemicals presented in Table 3. During the CFCG tests, the pH level of seawater was constantly monitored and maintained between 8.0 and 8.2, and fresh water was made once the level dropped below 8.0. The full CFCG test set-up is shown in Fig. 3. An environmental seawater chamber was attached onto the Instron machine, and the specimen was immersed in artificial seawater with the crack path located below the waterline throughout the tests (Fig. 3). The prepared seawater was stored in a water tank and circulated in the environmental chamber by means of a pump at a constant rate of 4 L/min. The seawater temperature was controlled with a chiller and maintained between 8.0 and 10.0 °C, to replicate the operation conditions in the North Sea [3].

3.2. Crack growth estimation method

During corrosion-fatigue tests, the specimens are immersed in seawater with limited direct access; therefore, the crack growth monitoring becomes challenging. One of the existing well-known and efficient crack growth monitoring techniques which is suitable for the CFCG testing is the back face strain (BFS) method that was designed for C(T) specimens [24,25]. The main idea for this approach

Table 1
Chemical composition of ER100S-1 material (wt.-%) [16].

	C	*Mn*	*Cr*	*Si*	*Ni*	*Mo*
ER100S-1	0.08	1.70	0.20	0.60	1.50	0.50

Table 2
CMT-WAAM fabrication parameters.

Shielding gas	Ar + 20% CO_2
Gas flow rate	15 L/min
Wire diameter	1.2 mm
Wire feed speed	7.5 m/min
Robot travelling speed	7.33 mm/sec
Dwell time	120 sec

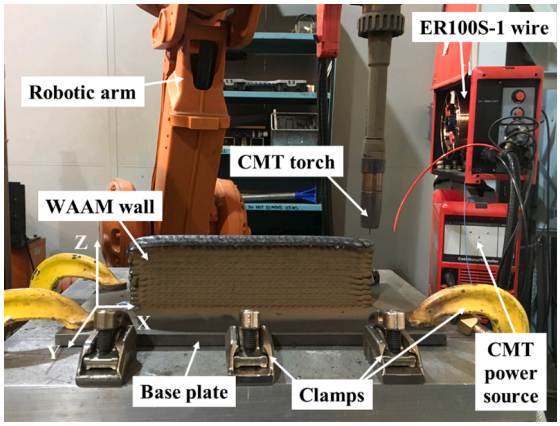

Fig. 1. Fabrication process including the CMT WAAM set-up and completed WAAM wall.

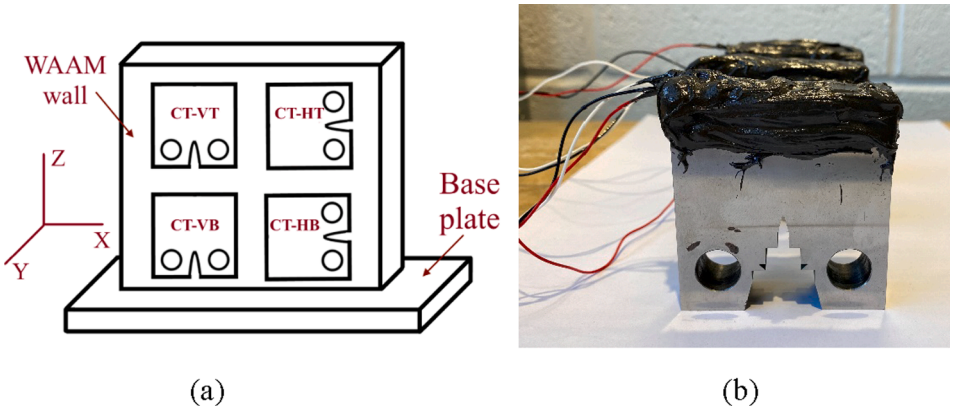

Fig. 2. (a) Specimen extraction plan from the WAAM wall, (b) specimens with protective coating after strain gauging.

Table 3
Chemical composition of artificial seawater [23].

Chemical compound	Concentration (g/L)
NaCl	24.53
$MgCl_2$	5.20
Na_2SO_4	4.09
$CaCl_2$	1.16
KCl	0.695
$NaHCO_3$	0.201
KBr	1.101
H_3BO_3	0.027
$SrCl_2$	0.025
NaF	0.003

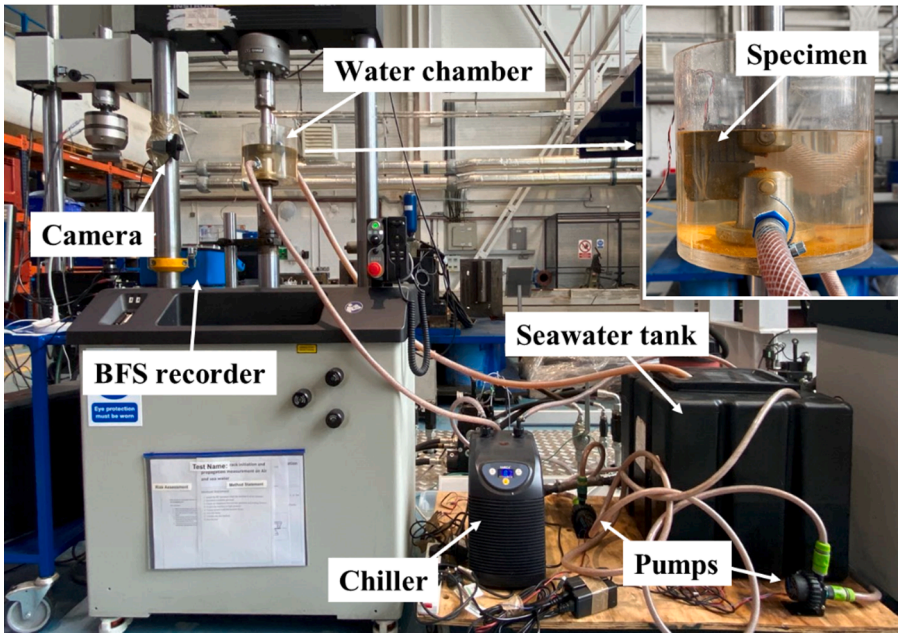

Fig. 3. CFCG test set-up.

is to correlate the BFS variations with the crack length of the specimen. The BFS calibration curve is initially developed under the same loading conditions during the FCG tests in air, where it is possible to measure the instantaneous crack length using the optical and compliance techniques. This calibration curve will be valid for the considered C(T) specimen geometry, material and loading conditions. Therefore, the same empirical correlation from FCG tests in air is used to estimate the crack lengths from the BFS measurements in CFCG tests in seawater.

The BFS values are recorded from the strain gauge attached to the back face of the C(T) specimen, at mid-height and mid-width. In this study, strain gauges were initially attached to the back face of C(T) specimens and then covered with a layer of a polysulfide coating to protect them against seawater damage (Fig. 3(b)). Prior to testing all the specimens were soaked in artificial seawater for approximately 24 h, as recommended in the ASTM D1141 [23] standard. The BFS values were recorded from the strain gauges every second by a strain recorder during the CFCG tests, and the maximum magnitude of compressive strain values were captured and stored on a memory card (see BFS recorder in Fig. 3(a)).

In order to produce unique BFS calibration curves for each specimen, four fatigue tests in air were carried out on C(T) specimens with the same geometry and extraction orientation/locations (VT, HT, VB, and HB). As the BFS calibration curves depend on the load level applied on the specimen during the test, the calibration test in air and the main CFCG test in seawater were performed at the same loading conditions as shown in Table 4. The instantaneous crack growth during the FCG test in air was measured using a clip gauge attached to the knife edges at the crack mouth of the C(T) specimens, and then correlated with the corresponding maximum magnitude of compressive BFS value (hence maximum crack mouth opening). Four calibration curve equations were derived by applying cubic polynomial lines of best fit to the experimental data, and then were used to estimate the crack length from the BFS measurements collected during each of the CFCG tests.

Additionally, to cross-check the accuracy of the estimated values of the crack length from the BFS method, the beach marking (BM) technique was employed in crack growth tests [26]. For this purpose, the maximum cyclic fatigue load and the frequency were decreased for a short period of time to introduce a thin mark on the fracture surface, which is called a beach mark. The duration of BM process was selected in such a way that it is performed without a noticeable crack growth, to keep the BFS value unchanged. By recording the BFS value at which the BM process was implemented, the estimated crack length from BFS method can be verified against the experimentally measured crack length at the BM line on the fracture surface of the opened C(T) specimen upon completion of the test. The BM loading conditions for seawater tests are presented in Table 4. For each CFCG test, the BM process was repeated three times at various stages of the test to build extra confidence in the developed BFS calibration curves. The BM method was first applied

Table 4
The loading condition during the main phase and beach marking phase of the calibration tests in air and CFCG tests in seawater.

Test environment	The main test condition			Beach marking loading condition		
	P_{max} (kN)	R	f (Hz)	P_{max} (kN)	R	f (Hz)
Air	10	0.1	5	8	0.125	3
Seawater	10	0.1	0.3	8	0.125	0.1

during the FCG tests in air on nominally identical C(T) specimens, to verify the accuracy of the crack length estimations, an example of the fracture surface and loading conditions are shown in Fig. 4 and Table 4 respectively. Satisfactory results from the air tests confirmed the accuracy of the compliance approach which was then implemented in CFCG tests.

Upon completion of the CFCG tests, all C(T) specimens were broken open to measure the actual crack length at BM lines on the fracture surfaces and verify the accuracy of the estimated crack lengths obtained from the BFS calibration curves. The fracture surfaces of four CFCG test specimens are presented in Fig. 5. It is worth noting here, that due to corroded fracture surface of the C(T) specimens tested in seawater, the beach marks were not very clear with the naked eye, compared with the fracture surfaces of the specimens tested in air (see Fig. 4), therefore high magnification optical microscopy was used to find the exact location of the BM lines. It can be seen in Fig. 5 that the crack propagation regions are symmetric in all CFCG specimens, indicating good alignment in the test set-up.

An example of the calibration curve for CT-VT specimen, plotted using the empirical correlation equation from the air test is presented in Fig. 6. Also included in this figure are the BM data points obtained at different stages of the test which indicate the actual crack lengths observed on the fracture surface upon the test completion and specimen fracture open. A very good agreement between the BFS calibration curve derived from the test in air and the BM data obtained from the CFCG test in seawater can be seen in this figure. Similar level of agreement between the calibration curves and the BM data points from the CFCG tests were obtained from the other three specimens (CT-VB, CT-HT, CT-HB). Hence the estimated crack lengths using the BFS data in CFCG tests are found to be very reliable.

3.3. Data analysis

The CFCG rates, da/dN, were determined using the estimated crack lengths and the experimental number of cycles for each specimen, by applying the secant method for the first and the last three data points, and seven-point incremental polynomial method for the rest of the data points. Subsequently, the stress intensity factor (SIF) was calculated using the shape function equation introduced by Mehmanparast et al. [27], Equation (1), which provides accurate solutions for a wider range of crack lengths in a C(T) specimen ranging between a/W of 0.2 and 0.7, compared with the original shape function equation from the ASTM E647 standard. In Equation (1), α is the normalised crack length a/W and ΔP is the load range which is defined as the difference between the maximum load P_{max} and the minimum load P_{min}.

$$\Delta K = \frac{\Delta P}{B\sqrt{W}} \bullet \frac{(2+\alpha)}{(1-\alpha)^{\frac{3}{2}}} \bullet (-372.12\alpha^6 + 1628.60\alpha^5 - 2107.46\alpha^4 + 1304.65\alpha^3 - 391.20\alpha^2 + 54.81\alpha + 7.57) \quad (1)$$

4. Experimental results and discussion

To assess and compare the duration of each test, the estimated crack lengths are plotted against the number of fatigue cycles for each specimen, and the results are displayed in Fig. 7. According to this figure, the longest fatigue life was experienced by the vertical specimen extracted from the top of the WAAM wall, CT-VT. This specimen required 1.5 to 2.6 times more cycles to propagate the crack by 15 mm than the other three specimens. Also seen in this figure is that the two specimens extracted from the top of the wall with two different orientations had the longest fatigue lives compared to specimens extracted from the bottom of the WAAM wall. For both locations of the WAAM wall considered in this study (i.e. top and bottom), the test duration for the vertical specimens is higher than the horizontal specimens extracted from the same location. Based on these experimental observations, the horizontal specimen extracted from the bottom of the wall, CT-HB, has the shortest fatigue life. These variations in the test duration are expected to have been caused by microstructural differences due to the thermal effects and possibly the remnant residual stresses which might have remained in the C(T) specimens after extraction. Additive layers at the bottom of the wall experience a greater number of repeated thermal cycles; therefore, it is expected that the magnitude of residual stress is generally lower at the bottom compared to the top of the WAAM wall.

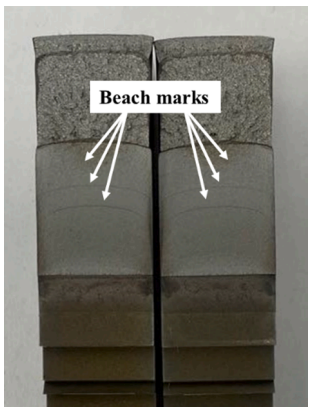

Fig. 4. The beach marks on fracture surface of WAAM ER100S-1C(T) specimen tested in air for development of BFS calibration curves.

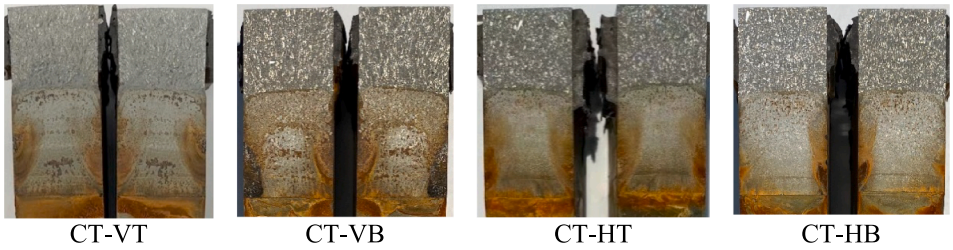

Fig. 5. Fracture surface of WAAM built ER100S-1 specimens after CFCG test in seawater.

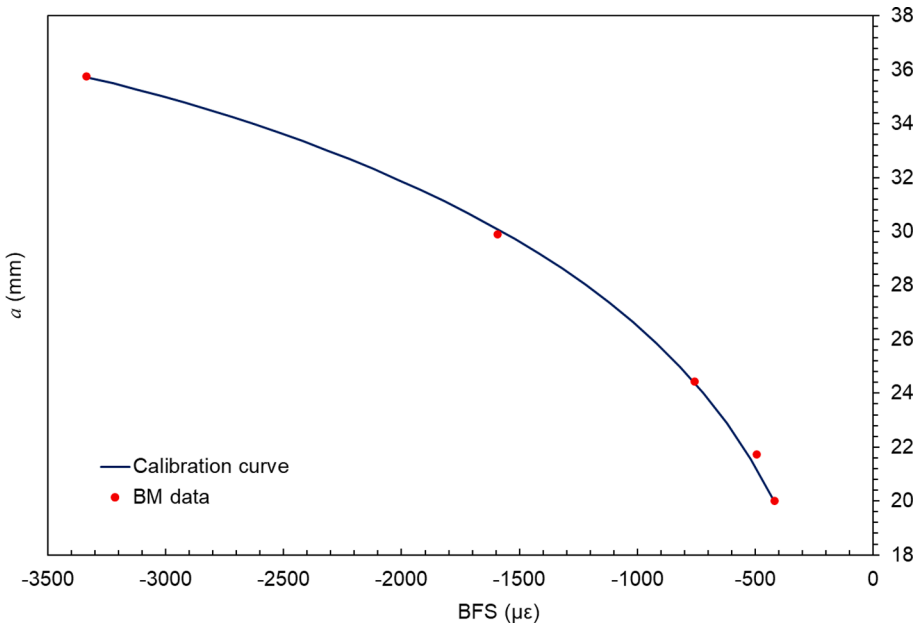

Fig. 6. Crack length vs. BFS correlation for CT-VT specimen, and its comparison with the BM data points.

Comparison of the CFCG data obtained from this study with the FCG results in air previously conducted on WAAM ER100S-1 specimens by Ermakova et al. [28] shows that in both test environments the crack growth results are sensitive to the extraction location, with a longer fatigue life experienced by the specimens extracted from the top of the WAAM wall.

The CFCG rates, *da/dN,* were calculated and plotted against the linear elastic fracture mechanic parameter, ΔK, as shown in Fig. 8. It can be observed in this figure that at the low values of ΔK, the crack growth rate is higher in horizontal specimens regardless of the extraction location; however, towards the end of the test, at larger values of ΔK, vertical specimens exhibit higher crack growth rates. In general, the lowest CFCG trend observed throughout the entire range of ΔK values is found to be obtained from CT-VT vertical specimen extracted from the top of the wall, indicating the highest level of corrosion-fatigue resistance across all four specimens considered in this study. Also seen in Fig. 8 is that within the inherent experimental scatter similar slopes are found in the CFCG trends from specimens with the same orientation. Moreover, the crack growth rates for vertical specimens show higher scatter than horizontal specimens, and display wavy patterns, similar to the observations reported by Ermakova et al. [28] for FCG tests on the same material and the same specimen orientation in air. It was also seen that the FCG rates from air test are location dependant, with the lowest crack growth rates observed in specimen extracted from the top of the wall. Thus, a conclusion can be made that for ER100S-1 WAAM built specimens, regardless of the testing environment, FCG and CFCG rates and test duration strongly depend on the extraction location. Having said that, considering that only four specimens were tested in seawater in the present study, more tests need to be conducted in future work to confirm the provisional results presented in this paper and assess the level of scatter for each specimen orientation and location. Furthermore, the remaining residual stresses in the C(T) specimens extracted from the WAAM wall must be measured in future work to evaluate their possible effects on the CFCG behaviour of ER100S-1 WAAM built specimens.

The CFCG test data were further analysed to evaluate the material constants, C and m (see Equation (2)), in the secondary Paris region for each dataset by plotting the lines of best fit to the experimental data and finding the corresponding power-law constants. The C and m values obtained from the regression analyses are presented in Table 5. Also included in this table are the values of coefficient of determination, R^2, to examine the level of scatter in each of the data sets. As seen in Table 5, the R^2 values for all specimens are close to 1, although a marginally higher level of scatter is generally observed in vertical specimens compared to the horizontal specimens.

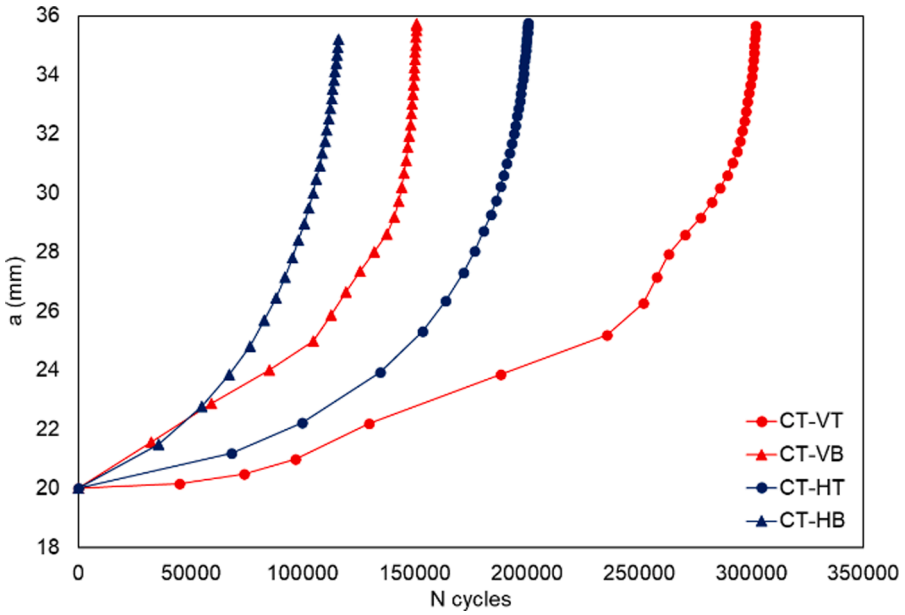

Fig. 7. Corrosion-fatigue crack growth trends in ER100S-1 WAAM built C(T) specimens.

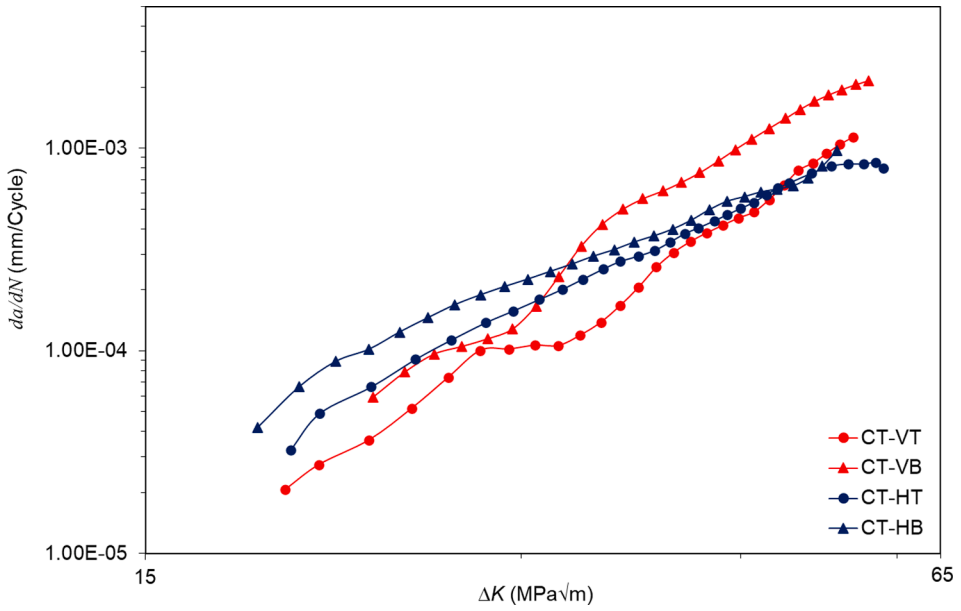

Fig. 8. Corrosion-fatigue crack growth results for ER100S-1 WAAM built specimens.

$$da/dN = C\Delta K^m \tag{2}$$

Furthermore, the power-law constants were determined for specimens with the same orientations (vertical or horizontal) and the results are presented in Table 6. Moreover, the upper bound trends for the vertical data set (Set-V) and horizontal data set (Set-H), based on +2 standard deviation (2SD), were calculated, and added to Table 6 and plotted in Fig. 9. Also shown in Fig. 9 is the comparison of the results obtained from this study with the recommended trends provided in the BS7910 standard for welded joints in seawater, based on the simplified law and the 2-stage law [29]. It can be seen in Fig. 9 that the upper bound trends for Set-V and Set-H from the CFCG tests on ER100S-1 WAAM built specimens both fall below the BS7910 recommended lines, except the very end of the Set-V, which crosses the 2-stage law at large values of ΔK. This indicates that the CFCG rates for ER100S-1 WAAM built specimens can be conservatively predicted by the simplified law provided in BS7910 standard.

Furthermore, the obtained CFCG results in this study have been compared with the experimental data available in the literature on

Table 5
Paris-law constants obtained from the CFCG test data on ER100S-1 WAAM built specimens (da/dN in mm/Cycle and ΔK in MPa $\sqrt{m}$).

Specimen ID	Orientation	Location	*Pmax* (kN)	*C*	*m*	R^2
CT-VT	Vertical	Top	10	2.89×10^{-10}	3.76	0.988
CT-VB	Vertical	Bottom	10	1.33×10^{-10}	4.15	0.987
CT-HT	Horizontal	Top	10	1.07×10^{-8}	2.82	0.995
CT-HB	Horizontal	Bottom	10	5.28×10^{-8}	2.44	0.994

Table 6
Power-law constants associated with the mean curves and upper bound trends for different specimen orientation datasets.

Datasets	Orientation	P_{max} (kN)	Mean			Mean + 2SD	
			C	*m*	R^2	*C*	*m*
Set-V	Vertical	10	1.49×10^{-10}	4.03	0.913	3.09×10^{-10}	4.03
Set-H	Horizontal	10	2.91×10^{-8}	2.58	0.972	3.77×10^{-8}	2.58

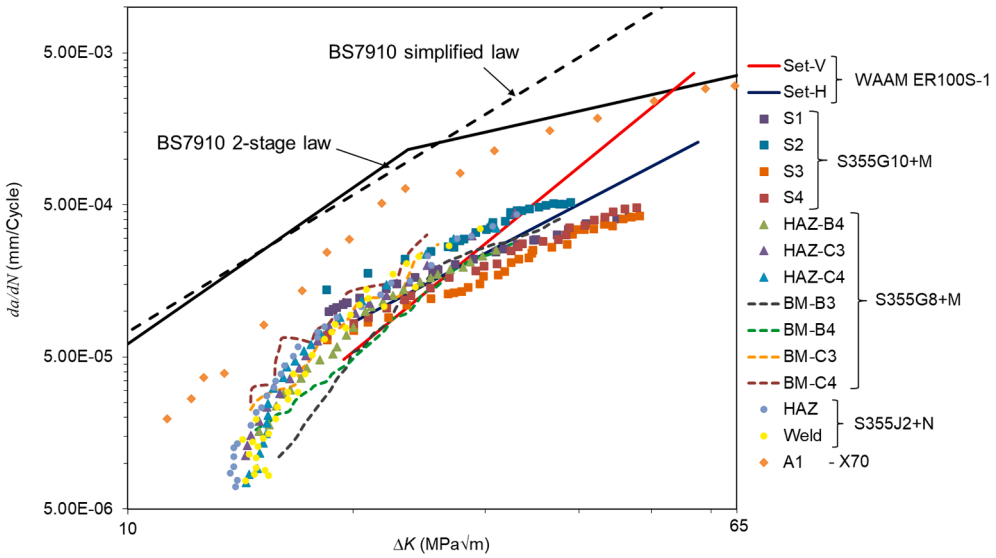

Fig. 9. Comparison of the upper bound CFCG trends for ER100S-1 WAAM built specimens with BS7910 curves and the literature data on structural steels.

conventionally built welded steel specimens tested in seawater, including: S355G8+M C(T) specimens extracted from HAZ and base metal [6], S355G10+M C(T) specimens extracted from HAZ [30], S355J2+N C(T) specimens extracted from HAZ and weld metal [1], and X70 pipeline steel specimens [31]. All specimens were tested under similar loading conditions as the samples tested in this study (see Table 4), and their trends are depicted in Fig. 9. Comparison of all considered datasets shows that the upper bound CFCG data obtained on ER100S-1 WAAM built specimens from the present study begins at approximately the same ΔK value as experimental data for S355G10+M specimens, though with a longer fatigue life, continuing to the higher values of ΔK. For the ΔK values of between approximately 19 and 35 MPa$\sqrt{m}$, the upper bound lines for ER100S-1 WAAM built specimens fall upon the test data on S355G10+M and S355G8+M, which are the subgrades of S355 structural steel that are widely used in fabrication of offshore renewable energy structures. Further comparison of the test durations for the specimens from this study and S355G+10 M HAZ specimens tested by Jacob et al. [30] shows that on average it takes 9.7 times longer to propagate a crack in WAAM ER100S-1 specimens than in conventionally welded S355 counterpart. Therefore, this comparison confirms that ER100S-1 steel and WAAM technology can be potentially considered for manufacturing of offshore renewable energy structures. Nevertheless, the S-N fatigue tests will need to be conducted in future work to fully assess the design requirements and structural integrity of WAAM built components operating under cyclic loading conditions in marine environments.

5. Fractography

Once four test specimens were broken-open, their fracture surfaces were examined using a TESCAN VEGA 3 Scanning Electron Microscope (SEM) with a magnification of 5000. According to Fig. 8, at lower values of ΔK the CFCG rates demonstrate higher level of

scatter; therefore, the microstructural analysis was conducted on the area corresponding to the beginning of the test (ΔK of approximately 23 MPa $\sqrt{\text{m}}$), and the results are shown in Fig. 10. The fracture surface examination in the regions shown in Fig. 10 demonstrates the existence of transgranular tortuous features for all specimens extracted with different orientations and locations, indicating a ductile fracture mechanism. Moreover, the general observation across various regions on the fracture surface shows that tortuosity of the vertical specimens is more pronounced, and deeper and larger in size, compared to the horizontal specimens which have smoother surface with shallower features. This indicates that at a given value of ΔK the CFCG would be higher in the horizontal specimens than the vertical samples. This conclusion is consistent with the trends presented in Fig. 8. Similar to the observations in the previous study on the FCG behaviour of WAAM built ER100S-1 specimens in air [28], elongated fracture features, which are marked with red dashed lines in Fig. 10, can be found in the vertical CFCG test specimens examined in this study both at the top and bottom locations (CT-VT and CT-VB). It was reported in the previous study [28] that once the orientation of these elongated fracture features changes, which appears with an increase in the inclination angle from the crack growth propagation plane, the FCG rate simultaneously increases. It is seen in Fig. 10 that the elongated fracture features in CT-VB have higher inclination angle, and hence higher CFCG rate than in CT-VT, where the feature is nearly parallel to the crack propagation direction, resulting in lower CFCG rate at a given value of ΔK as seen in Fig. 8. Comparison of two fracture surfaces of horizontal specimens shows that the specimen extracted from the bottom of the WAAM wall has shallower ductile features with higher density of small secondary cracks (shown with yellow arrows), whereas the fracture surface of the specimen extracted from the top of the wall exhibits deeper dimples and larger secondary cracks with lower density, which results in lower CFCG rates in CT-HT sample compared to CT-HB, which is confirmed by the trends observed in Fig. 8. Therefore, it can be concluded that for a given specimen orientation, the sample extracted from the bottom of the ER100S-1 WAAM wall exhibits less ductile fracture features, which result in higher CFCG rates compared to the top specimens.

6. Conclusions

The CFCG behaviour of ER100S-1 WAAM built specimens was investigated in the present study, the following conclusions and observations were made:

- The specimen extraction location with respect to the WAAM wall height has a major effect on the test duration and CFCG rates. Specimens extracted from the top of the wall require a greater number of cycles to propagate the crack and also demonstrate lower CFCG rates.
- Vertical specimens show a longer test duration compared to horizontal specimens extracted from the same location of WAAM wall, and on average they present lower CFCG rates.

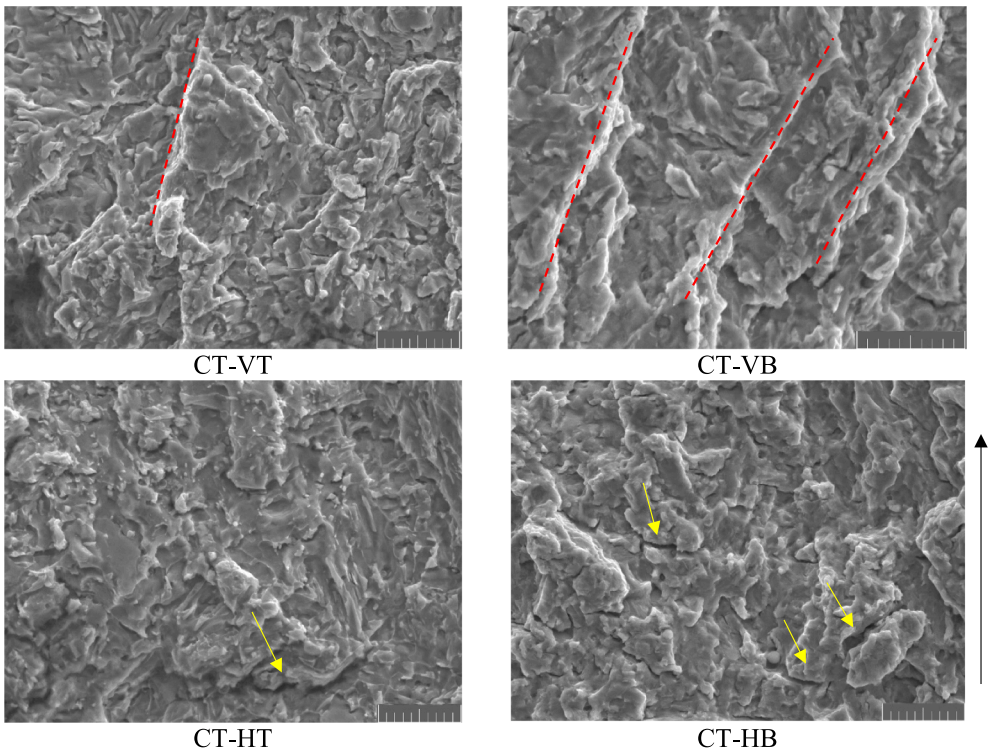

Fig. 10. SEM images of fracture surfaces for four test specimens at $\Delta K = 23$ MPa $\sqrt{\text{m}}$ (the scale bar is 10 μm, and the right-hand side arrow shows the direction of the crack propagation).

- The upper bound lines for CFCG trends fall below BS7910 recommended crack growth trends, and are on top of the existing test data on S355G10+M and S355G8+M.
- The ER100S-1 WAAM built specimens require on average 9.7 times greater number of cycles to propagate the crack by 15 mm compared to the wrought counterparts extracted from S355G10+M HAZ steel.
- Bottom portion of ER100S-1 WAAM steel wall represented a lower ductility, which subsequently results in higher CFCG rates.
- The fracture surface of the vertical WAAM built ER100S-1 specimens demonstrates elongated failure features. The higher inclination angle from the crack propagation plane results in a higher CFCG rate.
- Repeat tests are required in future work to evaluate the level of scatter for each specimen extraction location and orientation. Also, the remnant residual stresses in WAAM built C(T) specimens need to be measured to assess their potential effects on CFCG behaviour of ER100S-1 WAAM specimens.

Declaration of Competing Interest

The authors declare that they have no known competing financial interests or personal relationships that could have appeared to influence the work reported in this paper.

Acknowledgements

This work was supported by grant EP/L016303/1 for Cranfield, Oxford and Strathclyde Universities' Centre for Doctoral Training in Renewable Energy Marine Structures – REMS CDT (http://www.rems-cdt.ac.uk/) from the UK Engineering and Physical Sciences Research Council (EPSRC).

References

[1] O. Adedipe, F. Brennan, A. Mehmanparast, A. Kolios, I. Tavares, Corrosion fatigue crack growth mechanisms in offshore monopile steel weldments, Fatigue Fract. Eng. Mater. Struct. 40 (2017) 1868–1881.
[2] O.H. Burnside, S.J. Hudak Jr., E. Oelkers, K. Chan, R. Dexter. Long-Term Corrosion Fatigue of Welded Marine Steels. (1984).
[3] O. Adedipe, F. Brennan, A. Kolios, Review of corrosion fatigue in offshore structures: present status and challenges in the offshore wind sector, Renew. Sustain. Energy Rev. 61 (2016) 141–154.
[4] Fatigue behaviour of high-strength steel-welded joints in offshore and marine systems (FATHOMS) - Publications Office of the EU. https://op.europa.eu/en/publication-detail/-/publication/52679314-1c6d-41d6-9d70-19711b29427f.
[5] L. Bertini, Influence of seawater and residual stresses on fatigue crack growth in CMn steel weld joints, Theor. Appl. Fract. Mech. 16 (2) (1991) 135–144.
[6] A. Mehmanparast, F. Brennan, I. Tavares, Fatigue crack growth rates for offshore wind monopile weldments in air and seawater: SLIC inter-laboratory test results, Mater. Des. 114 (2017) 494–504.
[7] X. Zhang, et al., Fatigue Crack Growth in Additive Manufactured Titanium: Residual stress control and life evaluation method development. 29th ICAF Symposium-Nagoya 7–9, 2017.
[8] F. Martina, J. Mehnen, S.W. Williams, P. Colegrove, F. Wang, Investigation of the benefits of plasma deposition for the additive layer manufacture of Ti–6Al–4V, J. Mater. Process. Technol. 212 (6) (2012) 1377–1386.
[9] S.W. Williams, F. Martina, A.C. Addison, J. Ding, G. Pardal, P. Colegrove, Wire + arc additive manufacturing, Mater. Sci. Technol. 32 (7) (2016) 641–647.
[10] M. Rafieazad, A.V. Nemani, M. Ghaffari, A. Nasiri, On microstructure and mechanical properties of a low-carbon low-alloy steel block fabricated by wire arc additive manufacturing, J. Mater. Eng. Perform. 30 (7) (2021) 4937–4945.
[11] C.D.M. Liljedahl, J. Brouard, O. Zanellato, J. Lin, M.L. Tan, S. Ganguly, P.E. Irving, M.E. Fitzpatrick, X. Zhang, L. Edwards, Weld residual stress effects on fatigue crack growth behaviour of aluminium alloy 2024–T351, Int. J. Fatigue 31 (6) (2009) 1081–1088.
[12] X. Xu, S. Ganguly, J. Ding, S. Guo, S. Williams, F. Martina, Microstructural evolution and mechanical properties of maraging steel produced by wire + arc additive manufacture process, Mater. Charact. 143 (2018) 152–162.
[13] Ron, Levy, Dolev, Leon, Shirizly, Aghion, Environmental behavior of low carbon steel produced by a wire arc additive manufacturing process, Metals 9 (8) (2019) 888.
[14] T. Ron, O. Dolev, A. Leon, A. Shirizly, E. Aghion, Effect of phase transformation on stress corrosion behavior of additively manufactured austenitic stainless steel produced by directed energy deposition, Materials 14 (2021) 1–12.
[15] T. Ron, G.K. Levy, O. Dolev, A. Leon, A. Shirizly, E. Aghion, The effect of microstructural imperfections on corrosion fatigue of additively manufactured ER70S-6 alloy produced by wire arc deposition, Metals 10 (1) (2020) 98.
[16] *ER100S-G Data Sheet - Bohler Welding.* www.voestalpine.com/welding (2014).
[17] A. Ermakova, A. Mehmanparast, S. Ganguly, A review of present status and challenges of using additive manufacturing technology for offshore wind applications, Procedia Struct. Integrity 17 (2019) 29–36.
[18] A. Ermakova, A. Mehmanparast, S. Ganguly, J. Razavi, F. Berto, Investigation of mechanical and fracture properties of wire and arc additively manufactured low carbon steel components, *Theor. Appl. Fract. Mech.* 109 (2020), 102685.
[19] ASTM E647−13. Standard Test Method for Measurement of Fatigue Crack Growth Rates. *American Society for Testing and Materials* 1–50 (2014) doi:10.1520/E0647-15E01.2.
[20] American Society for Testing and Materials. ASTME-1820-11: standard test method for measurement of fracture toughness. *Annual book of ASTM standards* 1–55 (2011) doi:10.1520/E1820-18.
[21] Henderson, A. Hydrodynamic Loading of Offshore Wind Turbines. (2003).
[22] A. Jacob, A. Mehmanparast, R. D'Urzo, J. Kelleher, Experimental and numerical investigation of residual stress effects on fatigue crack growth behaviour of S355 steel weldments, *Int. J. Fatigue* 128 (2019), 105196.
[23] A. International, D1141–98 Standard Practice for the Preparation of Substitute Ocean Water, ASTM Int. 98 (2013) 1–3.
[24] O. Adedipe, F. Brennan, A. Kolios, Corrosion fatigue load frequency sensitivity analysis, Mar. Struct. 42 (2015) 115–136.
[25] J.C. Newman, Y. Yamada, M.A. James, Back-face strain compliance relation for compact specimens for wide range in crack lengths, Eng. Fract. Mech. 78 (15) (2011) 2707–2711.
[26] C. Hou, Fatigue analysis of welded joints with the aid of real three-dimensional weld toe geometry, Int. J. Fatigue 29 (4) (2007) 772–785.
[27] A. Mehmanparast, J. Taylor, F. Brennan, I. Tavares, Experimental investigation of mechanical and fracture properties of offshore wind monopile weldments: SLIC interlaboratory test results, Fatigue Fract. Eng. Mater. Struct. 41 (12) (2018) 2485–2501.
[28] A. Ermakova, S. Ganguly, J. Razavi, F. Berto, A. Mehmanparast, Experimental investigation of the fatigue crack growth behavior in wire arc additively manufactured ER100S-1 steel specimens, Fatigue Fract. Eng. Mater. Struct. 45 (2) (2022) 371–385.

[29] BS 7910. BSI Standards Publication Guide to methods for assessing the acceptability of flaws in metallic structures. *BSI Standards Publication* 490 (2015).
[30] A. Jacob, A. Mehmanparast, Crack growth direction effects on corrosion-fatigue behaviour of offshore wind turbine steel weldments, *Mar. Struct.* 75 (2021), 102881.
[31] K.C. Lieb, R.T. Horstman, B. Power, R.L. Meltzer, M.B. Vieth, O. Vosikovsky, Effects of stress ratio on fatigue crack growth rates in X70 pipeline steel in air and saltwater, J. Test. Eval. 8 (2) (1980) 68.